Three-photon light-sheet fluorescence microscopy

ADRIÀ ESCOBET-MONTALBÁN[1,†], PENGFEI LIU[1,†], JONATHAN NYLK[1], FEDERICO M. GASPAROLI[1], ZHENGYI YANG[1,+], AND KISHAN DHOLAKIA[1,*]

[1] *SUPA, School of Physics and Astronomy, University of St Andrews, North Haugh, Fife, KY16 9SS*
[+] *Present address: electron Bio-Imaging Centre, Diamond Light Source, Harwell Science and Innovation Campus, Didcot, OX11 0DE, UK*
[*] *Corresponding author: kd1@st-andrews.ac.uk*

Compiled May 16, 2018

We present the first demonstration of three-photon excitation light-sheet fluorescence microscopy. Light-sheet fluorescence microscopy in single- and two-photon excitation modes has emerged as a powerful wide-field, low photo-damage technique for fast volumetric imaging of biological samples. We extend this imaging modality to the three-photon regime enhancing its penetration depth. Our present study uses a standard femtosecond pulsed laser at 1000 nm wavelength for the imaging of 450 µm diameter cellular spheroids. In addition, we show, through numerical simulations, the potential advantages in three-photon light-sheet microscopy of using propagation-invariant Bessel beams in preference to Gaussian beams.

OCIS codes: (110.0180) Microscopy; (190.4180) Multiphoton processes; (180.2520) Fluorescence microscopy; (180.4315) Nonlinear microscopy; (180.6900) Three-dimensional microscopy; (110.4100) Imaging through turbid media.

Over the last two decades, the field of fluorescence microscopy has witnessed remarkable developments including super-resolution and fast volumetric imaging among many other innovations. However, a key remaining challenge is to perform imaging in situations where the scattering of light limits the penetration and performance of standard optical microscopy. This is crucial for imaging minute details of live biological samples at depth, without compromising their viability.

To increase depth penetration, multiphoton microscopy has come to the fore particularly in the form of two-photon excitation (2-PE) microscopy which has become the approach of choice for *in vivo* imaging [1, 2]. Recently, three-photon excitation (3-PE) microscopy with either point scanning [3] or with temporal focusing [4] has been employed to excite fluorophores with close to diffraction limited resolution into biological tissue for a greater penetration depth. Compared to the standard single-photon excitation (1-PE) or 2-PE, 3-PE has several benefits: the use of longer wavelengths reduces the effect of light scattering making it possible to increase the penetration depth of the illumination beam exciting deeper regions in the sample [3, 5]. Moreover, the nonlinear nature of the process confines the excitation to a smaller volume, reducing out-of-focus light as well as minimizing photo-bleaching on the biological sample [6, 7].

In parallel, the geometry used in light-sheet fluorescence microscopy (LSFM) has revolutionized the field of imaging by using a thin sheet of light to optically section samples which are typically transparent. In this technique, fluorescent light emitted by the sample is collected by a detection imaging system that is perpendicular to the illuminated plane. This particular configuration results in improved contrast and high axial resolution with very short acquisition times because it avoids scanning a focused beam across the field-of-view (FOV) [8]. In addition, as only the plane of interest is illuminated during a single exposure, photo-toxicity is vastly reduced. This makes LSFM very attractive for long term live imaging of biomedical samples [9–12]. At the same time, the FOV can be increased in LFSM notably by using propagation invariant light fields such as Bessel and Airy beams [13–15]. Furthermore, LSFM produces a series well-registered images that are advantageous for three-dimensional reconstruction of the specimen [16, 17].

In this letter, we present the first demonstration of LSFM using 3-PE. Our goal in the present work is to provide an approach to achieve greater imaging depths for biomedical imaging and explore advantages over the 2-PE counterpart in this particular imaging mode. The majority of research in the field of 3-PE microscopy has been performed using ultrashort pulsed lasers in imaging windows centered around wavelengths of 1300 nm and 1700 nm [5, 18]. However, such lasers are not available in most biomedical laboratories and they are limited to the imaging of green and red fluorescent samples, respectively. In this study we use a standard Ti:Sapphire ultrashort pulsed laser normally used for 2-PE microscopy, to generate 3-PE of fluorophores with 1-PE absorption peaks in the violet and UV region of the spectrum ($\lambda < 400$ nm), including a PUREBLU™ Hoechst 33342 dye (Bio-Rad) and blue fluorescing polymer microspheres (B0100, 1 µm, Duke Scientific). The laser used in our investigation is a Coherent Chameleon Ultra II with tunable central wavelength between 680 nm and 1080 nm, with a 140 fs pulse duration and 80 MHz repetition rate.

It is well known that 3-PE is a nonlinear process in which the emitted fluorescence signal increases with the cube of the power of the illumination laser [19]. Based on this property, a simple initial experiment was designed to determine the presence of 3-PE fluorescence signal from the fluorophores used in this study. The

cubic dependence on laser power was confirmed by measuring the fluorescence emission intensity as the laser power was modulated at known steps. In order to find the optimum wavelength for 3-PE using a Ti:Sapphire laser, the fluorophores were tested at wavelengths ranging from 750 nm to 1050 nm. The brightest and most stable signals were observed at 1000 nm obtaining values of n = 2.96 ± 0.08 and n = 3.16 ± 0.03 for the blue fluorescing beads and PUREBLU™ Hoechst 33342 dye, respectively. Additionally, their emission spectra were measured and compared to 1-PE at a wavelength of 405 nm (56ICS/S2667, Melles Griot), showing good overlap and corroborating the presence of a 3-PE signal.

A digitally scanned light-sheet fluorescence microscope (DSLM) [20], based on the openSPIM geometry [21], was implemented for this investigation. The ultrashort pulsed laser beam was expanded to illuminate a single-axis galvanometric mirror (GVS011, Thorlabs) driven by a triangular wave of variable frequency and amplitude (TG 210, Aim-TTi). A virtual light-sheet was generated inside the sample chamber by relaying the scanning mirror onto the back aperture of the illumination objective (MRH07120, Nikon, 10x/0.3 numerical aperture (NA), 3.5 mm working distance (wd), water-dipping). Based on measurements of the beam size at the back aperture of the objective, the NA of the light-sheet was determined to be 0.17 ± 0.01. Power control was achieved by combining a half-wave plate (WPH05M-780, Thorlabs) mounted on a manual rotation mount (CRM1, Thorlabs) and a polarizing beam splitting cube (CM1-PBS252, Thorlabs). Samples were held from above and accurately positioned using a XYZ linear translation stage (M-562-XYZ, Newport). Stacks of images were acquired by stepwise motion of the sample across the light-sheet using a motorized actuator (M-230.10, PI). Fluorescence was collected perpendicularly to the illumination plane by a second objective lens (UMPLFLN 20XW, Olympus, 20x/0.5 NA, 3.5 mm wd, water-dipping). A 400 mm tube lens (AC254-400-A-ML, Thorlabs) focused the light on a water-cooled sCMOS camera (C11440-42U30, HAMAMATSU), yielding a magnification of 40x. Two fluorescence filters (FF01-680/SP, FF01-468/SP, Semrock) were used to block scattered light from the illumination laser and also reject possible undesired 2-PE signal emitted at longer wavelengths. The LSFM we have developed can be operated at 2-PE as well as at 3-PE by simply shifting the laser wavelength.

For showing the capability of 3-PE LSFM, our first demonstration imaged 1 µm diameter blue fluorescing beads embedded in 1.5 % agarose in a FEP (Fluorinated Ethylene Propylene) capillary. Stacks of images were acquired at steps of 0.25 µm and the performance of the system was compared to 2-PE. The laser power was adjusted for each experiment in order to achieve the same maximum intensity values on the camera in both imaging modalities to perform fair comparisons. The maximum laser power available at the back aperture of the illumination objective for the 3-PE experiments at 1000nm was 350 mW while in the 2-PE excitation experiments a power of 13 mW at a wavelength of 700 nm generated the same fluorescence intensity. Maximum intensity projections in the axial direction clearly show the intrinsic optical sectioning capability of LSFM (Fig. 1(a, b)).

The full width at half maximum (FWHM) of the point spread function (PSF) was measured in various images obtaining an axial resolution of 1.66 ± 0.10 µm and 1.59 ± 0.15 µm for 3-PE and 2-PE, respectively (Fig. 1(c)). Approximately, the same axial resolution is achieved in both modalities even using different illumination wavelengths due to the highly confined excitation of the 3-PE process. The FOV of a light-sheet microscope is usually

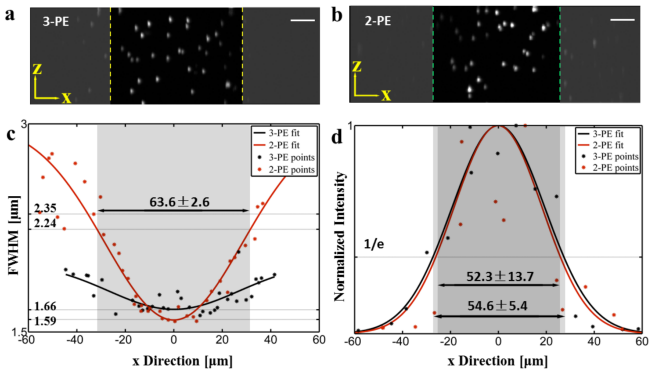

Fig. 1. Comparison between 2-PE and 3-PE LSFM. Axial maximum intensity projections of 3D stacks of images of 1 µm blue fluorescing microspheres embedded in agarose under (a) 3-PE at 1000 nm and (b) 2-PE at 700 nm. Scale bar, 10 µm. x-axis: beam propagation; z-axis: optical axis of detection lens. (c) Statistical estimates of the axial resolution and FOV based on FWHM. (d) Statistical estimate of the FOV based on normalized fluorescence intensity.

defined as the Rayleigh range of the illumination beam, i.e. the propagation range in which the beam width remains less than $\sqrt{2}$ times its minimum size. However, in 3-PE the light-sheet remains thin *enough* well beyond the expected Rayleigh range due to the properties of the higher order nonlinear excitation process. Consequently, the usable FOV was defined based on the edge-to-edge drop in fluorescence intensity in a 1/e-dependent manner (Fig. 1(d)). Furthermore, the tighter excitation confinement of 3-PE compared to 2-PE results in a much reduced out-of-focus fluorescence excitation along the propagation direction of the light-sheet. For instance, in 3-PE the usable FOV is 54.6± 5.4 µm while the total excited area is contained in 80 µm along the light-sheet. In contrast, in 2-PE the usable FOV is 52.3± 13.7 µm but the excited region extends up to 140 µm. It should also be noted that chromatic aberrations in the illumination path make the beam shift both transversally and longitudinally when switching between 3-PE and 2-PE. Such strong chromatic aberrations should be accounted for and corrected if simultaneous multicolor experiments are to be performed [22, 23].

The feasibility of using 3-PE LSFM for biomedical applications is demonstrated by imaging cellular spheroids of ≈ 450 µm in diameter. Human Embryonic Kidney cells (HEK 293 T17) were plated in an ultra-low attachment 96-well round bottom cell culture plate (Corning® Costar® 7007) and grown for 48 hours. When the spheroids were formed, their outer layer was labelled with the PUREBLU™ Hoechst 33342 nuclear staining dye (Fig. 2). Spheroids were embedded in 1% agarose in a FEP capillary. Stacks of images with 0.5 µm spacing were acquired and three-dimensional (3D) images where rendered to show the imaging capabilities of the presented microscope (Supplementary Video). Single 3-PE slices in the XY and YZ planes are shown in Fig. 2(b, c). In order to assess its performance at depth in scattering samples, the near and far surfaces of the spheroid with respect to the illumination light-sheet (blue and red rectangles in Fig. 2(a), respectively) were imaged first under 2-PE and then with 3-PE. Stacks were acquired with the same exposure time and the equivalent laser powers previously determined. Image quality was quantified by measuring the contrast-to-noise ratio (CNR) at various positions in the images [24]. Near the

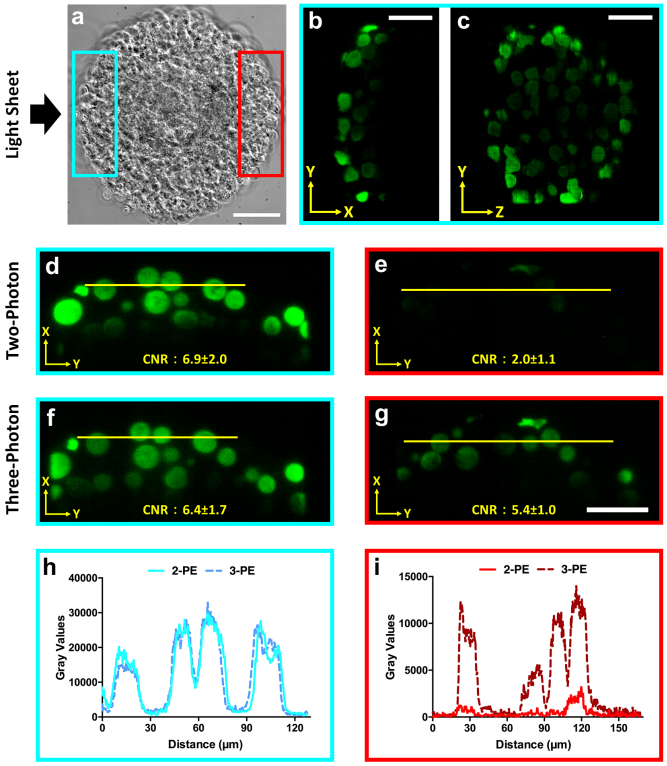

Fig. 2. HEK 293 T17 cellular spheroids labeled with PURE-BLU™ Hoechst 33342 nuclear staining dye imaged with 2-PE and 3-PE LSFM. (a) Brightfield image of a cellular spheroid (diameter ≈ 450 μm). The blue and red rectangles represent the near and far surfaces of the spheroid with respect to the light-sheet illumination direction (black arrow). (b, c) Single XY and YZ near-surface planes (blue rectangle in (a)) of a cellular spheroid imaged with 3-PE light sheet. (d-g) Single XY plane of a ≈ 450 μm cellular spheroid imaged with 2-PE (d, e) and 3-PE light-sheet in both the near (d, f) and far-surface (e, g). The 3D rendering of the image stacks acquired in both 2-PE and 3-PE can be found in the Supplementary Video (see **Visualization 1**). (h, i) Fluorescence intensity profiles along the yellow lines highlighted in (d-g). Brightfield image scale bar, 100 μm; Fluorescence images scale bar, 50 μm.

surface, both modalities show the same image quality with similar CNR values as shown in Fig. 2(d, f). However, at the far surface of the spheroid 2-PE shows a dramatic drop in image quality (Fig. 2(e)) while 3-PE still preserves high contrast due to the use of a longer wavelength (Fig. 2(g)). The CNR in 2-PE drops by approximately 71 % at a depth of nearly 450 μm while in 3-PE it only decreases by 15 %. Line profiles in Fig. 2(h, i) show the clear improvement in contrast of 3-PE compared to 2-PE in imaging at depth (see also **Visualization 1**).

To compare our results with theoretical expectations, light-sheet profiles for 1-, 2-, and 3-PE were numerically modeled using Fourier beam propagation. In all cases the following parameters were used: NA$= 0.17 \pm 0.01$, $\lambda_{n-PE} = n\lambda_{1-PE}$, with $\lambda_{1-PE} = 333$ nm.

Our simulations of Gaussian light-sheets predicted resolutions (given by the FWHM of the light-sheet profile) of 1.4 ± 0.1 and 1.7 ± 0.1 and FOV of 48 ± 6 μm and 58 ± 8 μm for 2- and 3-PE respectively, which is in close agreement with the experimental results.

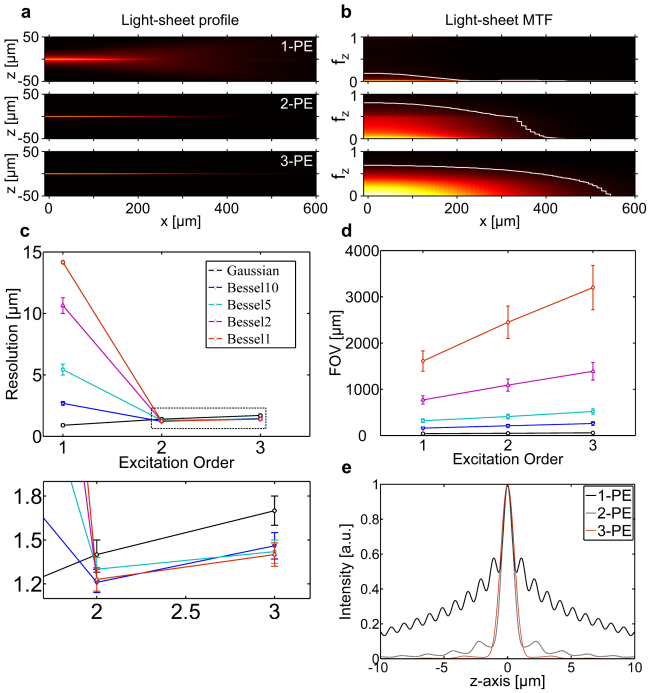

Fig. 3. Characterisation of 1-, 2-, and 3-PE LSFM with Bessel beam illumination. (a) XZ light-sheet cross-sections for 1-PE (top), 2-PE (middle), and 3-PE (bottom) of a Bessel5 beam and (b) their respective axial MTFs. The spatial frequency, f_z, is normalised to $2NA/\lambda_{1-PE}$ and the white lines indicate the isosurface at 5% contrast. (c) peak axial resolution and (d) FOV for a Gaussian light-sheet and Bessel light-sheets with $\beta = 1, 2, 5, 10$ in 1-, 2-, and 3-PE. Inset in (c) shows magnified view of the dashed box. (e) Transverse light-sheet cross-sections at 'focus' ($x = 0$) for 1-, 2-, and 3-PE.

Numerical models also facilitated exploration of other beam types for 3-PE light sheet. Bessel beams have been shown to have much better properties for light-sheet imaging in 2-PE than 1-PE [14, 25]. So we also compared Bessel beam illumination for 3-PE. Bessel beams were generated by a thin annulus in the pupil plane of the illumination objective [14]. We define Besselβ to denote a Bessel beam generated by an annular ring where β is the percentage thickness of the outer radius of the ring.

Figure 3(a) shows the cross-sectional light-sheet profiles for a Bessel5 beam in 1-, 2-, and 3-PE. Due to the extended transverse profile of the Bessel beam, it is not suitable to measure the FWHM to indicate resolution, therefore this was determined from the axial modulation transfer function, $MTF_z(f_z, x) = \mathcal{F}_z(LS(z, x))$, where $LS(x, z)$ is the light-sheet cross-section and $\mathcal{F}_z$ denotes the 1D Fourier transform along the axial direction (Fig. 3(b)). The MTF concisely represents information of both resolution and contrast. We set a practical noise-floor at 5% contrast to determine the maximum axial resolution, which is shown in Fig. 3(c). The FOV was determined from the $1/e$ points in the longitudinal intensity profile of the light-sheet (Fig. 3(d)). Figures 3(c,d) show that, for the same NA, 3-PE of a Bessel light-sheet has a slight reduction in resolution compared to 2-PE but greatly increases the FOV. It also shows that the resolution is effectively decoupled from the FOV as it exhibits very little change with β. This can be understood from looking at the cross-section

of the light-sheet. Figure 3(e) shows the transverse intensity profiles of the light-sheets in Fig. 3(a) at 'focus' ($x = 0$). For 1-PE, all the side-lobes contribute equal fluorescence as the central lobe and, when scanned to form the light-sheet, these blur into one another giving a broad profile. In 2-PE, the contributions of the side-lobes are reduced and the light-sheet profile is much more Gaussian in shape, although there is some extended structure. In 3-PE the contributions of the side-lobes are suppressed to a greater extent, and so increasing the propagation-invariant length of the beam (by decreasing β) will not significantly affect the resolution. This quantitative MTF study supports the more qualitative outcomes observed in recent works by Chen *et al.* [26] and Rodríguez *et al.* [27] which have shown improvements in lateral resolution and image quality when using a Bessel beam extended focus for 3-PE confocal microscopy.

In summary, we have demonstrated a new light-sheet fluorescence microscopy approach based on 3-PE that results in an extended imaging depth when compared with the currently available 2-PE light-sheet microscopy. By imaging $\approx 450\,\mu$m spheroids, we show that its performance at shallow depths is comparable to 2-PE imaging while at larger depths 3-PE clearly enables greater image contrast. From our simulations, we have shown that the combination of 3-PE with Bessel beam illumination will be even more advantageous for LSFM, achieving deeper penetration and a larger FOV while maintaining high resolution. Finally, the imaging depth could be further improved by using longer wavelengths and combining it with attenuation-compensation approaches recently developed for propagation-invariant fields [24].

Funding

This work has received funding from the European Union's Horizon 2020 Programme through the project Advanced BiomEdical OPTICAL Imaging and Data Analysis (BE-OPTICAL) under grant agreement no. 675512 and the UK Engineering and Physical Sciences Research Council (grants EP/P030017/1 and EP/R004854/1).

Acknowledgments

We thank David E. K. Ferrier and Frances Goff for providing samples, Stella Corsetti for assistance with characterization and Roman Spesyvtsev for contributions at early stages of the work.

†AEM and PL contributed equally to the work presented.

REFERENCES

1. W. Denk, J. H. Strickler, and W. W. Webb, Science **248**, 73-76 (1990).
2. G. Katona, G. Szalay, P. Maák, A. Kaszás, M. Veress, D. Hillier, B. Chiovini, E. S. Vizi, B. Roska, and B. Rózsa, Nat. Methods **9**, 201-208 (2012).
3. N. G. Horton, K. Wang, D. Kobat, C. G. Clark, F. W. Wise, C. B. Schaffer, and C. Xu, Nat. Photonics **7**, 205-209 (2013).
4. C. J. Rowlands, D. Park, O. T. Bruns, K. D. Piatkevich, D. Fukumura, R. K. Jain, M. G. Bawendi, E. S. Boyden, and P. T. So, Light. Sci. & Appl. **6**, e16255 (2016).
5. D. G. Ouzounov, T. Wang, M. Wang, D. D. Feng, N. G. Horton, J. C. Cruz-Hernández, Y.-T. Cheng, J. Reimer, A. S. Tolias, N. Nishimura, and C. Xu, Nat. Methods **14**, 388-390 (2017).
6. F. Helmchen and W. Denk, Nat. Methods **2**, 932-940 (2005).
7. D. L. Wokosin, V. E. Centonze, S. Crittenden, and J. White, Bioimaging **4**, 208-214 (1996).
8. J. Huisken, J. Swoger, F. Del Bene, J. Wittbrodt, and E. H. Stelzer, Science **305**, 1007-1009 (2004).
9. E. G. Reynaud, U. Kržič, K. Greger, and E. H. K. Stelzer, HFSP J. **2**, 266-275 (2008).
10. E. H. Stelzer, Mech. Dev. **126**, S36 (2009).
11. F. Pampaloni, N. Ansari, P. Girard, and E. H. Stelzer, Proc. SPIE **8086**, 80860Y (2011).
12. E. G. Reynaud, J. Peychl, J. Huisken, and P. Tomancak, Nat. Methods **12**, 30-34 (2015).
13. F. O. Fahrbach, V. Gurchenkov, K. Alessandri, P. Nassoy, and A. Rohrbach, Opt. Express **21**, 13824-13839 (2013).
14. T. Vettenburg, H. I. Dalgarno, J. Nylk, C. Coll-Lladó, D. E. Ferrier, T. Čižmár, F. J. Gunn-Moore, and K. Dholakia, Nat. Methods **11**, 541-544 (2014).
15. P. Piksarv, D. Marti, T. Le, A. Unterhuber, L. H. Forbes, M. R. Andrews, A. Stingl, W. Drexler, P. E. Andersen, and K. Dholakia, Sci. Rep. **7**, 1435 (2017).
16. R. Tomer, K. Khairy, F. Amat, and P. J. Keller, Nat. Methods **9**, 755-736 (2012).
17. H.-U. Dodt, U. Leischner, A. Schierloh, N. Jährling, C. P. Mauch, K. Deininger, J. M. Deussing, M. Eder, W. Zieglgänsberger, and K. Becker, Nat. Methods **4**, 331-336 (2007).
18. K. Guesmi, L. Abdeladim, S. Tozer, P. Mahou, T. Kumamoto, K. Jurkus, P. Rigaud, K. Loulier, N. Dray, P. Georges, M. Hanna, J. Livet, W. Supatto, E. Beaurepaire, and F. Druon, Light. Sci. Appl. (2018).
19. C. Xu, W. Zipfel, J. B. Shear, R. M. Williams, and W. W. Webb, Proc. Natl. Acad. Sci. **93**, 10763-10768 (1996).
20. P. J. Keller, A. D. Schmidt, J. Wittbrodt, and E. H. Stelzer, Science. **322**, 1065-1069 (2008).
21. P. G. Pitrone, J. Schindelin, L. Stuyvenberg, S. Preibisch, M. Weber, K. W. Eliceiri, J. Huisken, and P. Tomancak, Nat. Methods **10**, 598-599 (2013).
22. P. Mahou, G. Malkinson, É. Chaudan, T. Gacoin, E. Beaurepaire, and W. Supatto, Small **13**, 1701442 (2017).
23. P. Mahou, M. Zimmerley, K. Loulier, K. S. Matho, G. Labroille, X. Morin, W. Supatto, J. Livet, D. Débarre, and E. Beaurepaire, Nat. Methods **9**, 815 (2012).
24. J. Nylk, K. McCluskey, M. A. Preciado, M. Mazilu, Z. Yang, F. J. Gunn-Moore, S. Aggarwal, J. A. Tello, D. E. K. Ferrier, and K. Dholakia, Sci. Adv. **4**, eaar4817 (2018).
25. O. E. Olarte, J. Licea-Rodriguez, J. A. Palero, E. J. Gualda, D. Artigas, J. Mayer, J. Swoger, J. Sharpe, I. Rocha-Mendoza, R. Rangel-Rojo *et al.*, Biomed. Opt. Express **3**, 1492-1050 (2012).
26. B. Chen, X. Huang, D. Gou, J. Zeng, G. Chen, M. Pang, Y. Hu, Z. Zhao, Y. Zhang, Z. Zhou, H. Wu, H. Cheng, Z. Zhang, C. Xu, Y. Li, L. Chen, and A. Wang, Biomed. Opt. Express **9**, 1992-2000 (2018).
27. C. Rodríguez, Y. Liang, R. Lu, and N. Ji, Opt. Lett. **43**, 1914-1917 (2018).

REFERENCES

1. W. Denk, J. H. Strickler, and W. W. Webb, "Two-photon laser scanning fluorescence microscopy," Science. **248**, 73–76 (1990).
2. G. Katona, G. Szalay, P. Maák, A. Kaszás, M. Veress, D. Hillier, B. Chiovini, E. S. Vizi, B. Roska, and B. Rózsa, "Fast two-photon in vivo imaging with three-dimensional random-access scanning in large tissue volumes," Nat. Methods **9**, 201–208 (2012).
3. N. G. Horton, K. Wang, D. Kobat, C. G. Clark, F. W. Wise, C. B. Schaffer, and C. Xu, "In vivo three-photon microscopy of subcortical structures within an intact mouse brain," Nat. Photonics **7**, 205–209 (2013).
4. C. J. Rowlands, D. Park, O. T. Bruns, K. D. Piatkevich, D. Fukumura, R. K. Jain, M. G. Bawendi, E. S. Boyden, and P. T. So, "Wide-field three-photon excitation in biological samples," Light. Sci. & Appl. **6**, e16255 (2016).
5. D. G. Ouzounov, T. Wang, M. Wang, D. D. Feng, N. G. Horton, J. C. Cruz-Hernández, Y.-T. Cheng, J. Reimer, A. S. Tolias, N. Nishimura, and C. Xu, "In vivo three-photon imaging of activity of GCaMP6-labeled neurons deep in intact mouse brain," Nat. Methods **14**, 388–390 (2017).
6. F. Helmchen and W. Denk, "Deep tissue two-photon microscopy," Nat. Methods **2**, 932–940 (2005).
7. D. L. Wokosin, V. E. Centonze, S. Crittenden, and J. White, "Three-photon excitation fluorescence imaging of biological specimens using an all-solid-state laser," Bioimaging **4**, 208–214 (1996).
8. J. Huisken, J. Swoger, F. Del Bene, J. Wittbrodt, and E. H. Stelzer, "Optical sectioning deep inside live embryos by selective plane illumination microscopy," Science **305**, 1007–1009 (2004).
9. E. G. Reynaud, U. Kržič, K. Greger, and E. H. K. Stelzer, "Light sheet based fluorescence microscopy: More dimensions, more photons, and less photodamage," HFSP J. **2**, 266–275 (2008).
10. E. H. Stelzer, "S09-02 Light sheet based fluorescence microscopes (LSFM, SPIM, DSLM) reduce phototoxic effects by several orders of magnitude," Mech. Dev. **126**, S36 (2009).
11. F. Pampaloni, N. Ansari, P. Girard, and E. H. Stelzer, "Light sheet-based fluorescence microscopy (lsfm) reduces phototoxic effects and provides new means for the modern life sciences," Proc. SPIE **8086**, 80860Y (2011).
12. E. G. Reynaud, J. Peychl, J. Huisken, and P. Tomancak, "Guide to light-sheet microscopy for adventurous biologists," Nat. Methods **12**, 30-34 (2015).
13. F. O. Fahrbach, V. Gurchenkov, K. Alessandri, P. Nassoy, and A. Rohrbach, "Light-sheet microscopy in thick media using scanned bessel beams and two-photon fluorescence excitation," Opt. Express **21**, 13824–13839 (2013).
14. T. Vettenburg, H. I. Dalgarno, J. Nylk, C. Coll-Lladó, D. E. Ferrier, T. Čižmár, F. J. Gunn-Moore, and K. Dholakia, "Light-sheet microscopy using an airy beam," Nat. Methods **11**, 541–544 (2014).
15. P. Piksarv, D. Marti, T. Le, A. Unterhuber, L. H. Forbes, M. R. Andrews, A. Stingl, W. Drexler, P. E. Andersen, and K. Dholakia, "Integrated single-and two-photon light sheet microscopy using accelerating beams," Sci. Rep. **7**, 1435 (2017).
16. R. Tomer, K. Khairy, F. Amat, and P. J. Keller, "Quantitative high-speed imaging of entire developing embryos with simultaneous multiview light-sheet microscopy," Nat. Methods **9**, 755–763 (2012).
17. H.-U. Dodt, U. Leischner, A. Schierloh, N. Jährling, C. P. Mauch, K. Deininger, J. M. Deussing, M. Eder, W. Zieglgänsberger, and K. Becker, "Ultramicroscopy: three-dimensional visualization of neuronal networks in the whole mouse brain," Nat. Methods **4**, 331–336 (2007).
18. K. Guesmi, L. Abdeladim, S. Tozer, P. Mahou, T. Kumamoto, K. Jurkus, P. Rigaud, K. Loulier, N. Dray, P. Georges, M. Hanna, J. Livet, W. Supatto, E. Beaurepaire, and F. Druon, "Dual-color deep-tissue three-photon microscopy with a multiband infrared laser," Light. Sci. Appl. (2018).
19. C. Xu, W. Zipfel, J. B. Shear, R. M. Williams, and W. W. Webb, "Multiphoton fluorescence excitation: new spectral windows for biological nonlinear microscopy," Proc. Natl. Acad. Sci. **93**, 10763–10768 (1996).
20. P. J. Keller, A. D. Schmidt, J. Wittbrodt, and E. H. Stelzer, "Reconstruction of Zebrafish Early Embryonic Development by Scanned Light Sheet Microscopy," Science. **322**, 1065–1069 (2008).
21. P. G. Pitrone, J. Schindelin, L. Stuyvenberg, S. Preibisch, M. Weber, K. W. Eliceiri, J. Huisken, and P. Tomancak, "OpenSPIM: an open-access light-sheet microscopy platform," Nat. Methods **10**, 598-599 (2013).
22. P. Mahou, G. Malkinson, É. Chaudan, T. Gacoin, E. Beaurepaire, and W. Supatto, "Metrology of Multiphoton Microscopes Using Second Harmonic Generation Nanoprobes," Small **13**, 1701442 (2017).
23. P. Mahou, M. Zimmerley, K. Loulier, K. S. Matho, G. Labroille, X. Morin, W. Supatto, J. Livet, D. Débarre, and E. Beaurepaire, "Multicolor two-photon tissue imaging by wavelength mixing," Nat. Methods **9**, 815–818 (2012).
24. J. Nylk, K. McCluskey, M. A. Preciado, M. Mazilu, Z. Yang, F. J. Gunn-Moore, S. Aggarwal, J. A. Tello, D. E. K. Ferrier, and K. Dholakia, "Light-sheet microscopy with attenuation-compensated propagation-invariant beams," Sci. Adv. **4**, eaar4817 (2018).
25. O. E. Olarte, J. Licea-Rodriguez, J. A. Palero, E. J. Gualda, D. Artigas, J. Mayer, J. Swoger, J. Sharpe, I. Rocha-Mendoza, R. Rangel-Rojo *et al.*, "Image formation by linear and nonlinear digital scanned light-sheet fluorescence microscopy with gaussian and bessel beam profiles," Biomed. optics express **3**, 1492–1505 (2012).
26. B. Chen, X. Huang, D. Gou, J. Zeng, G. Chen, M. Pang, Y. Hu, Z. Zhao, Y. Zhang, Z. Zhou, H. Wu, H. Cheng, Z. Zhang, C. Xu, Y. Li, L. Chen, and A. Wang, "Rapid volumetric imaging with Bessel-Beam three-photon microscopy," Biomed. Opt. Express **9**, 1992–2000 (2018).
27. C. Rodríguez, Y. Liang, R. Lu, and N. Ji, "Three-photon fluorescence microscopy with an axially elongated Bessel focus," Opt. Lett. **43**, 1914–1917 (2018).